ISSN 1674-1056
http://cpb.iphy.ac.cn
http://iopscience.iop.org/cpb
中国物理 B
Chinese Physics
中国物理 Chinese Physics B

High common mode rejection ratio InP 90° optical hybrid in ultra-broadband at 60 nm with deep-rigded waveguide based on ×4 MMI coupler

Zi-Qing Lu(陆子晴), Qin Han(韩勤), Han Ye(叶焓), Shuai Wang(王帅), Feng Xiao(肖峰), Fan Xiao(肖帆)
Citation: Chin. Phys. B . 2020, 29(5): 054206 . **doi:** 10.1088/1674-1056/ab7b52
Journal homepage: http://cpb.iphy.ac.cn; http://iopscience.iop.org/cpb

What follows is a list of articles you may be interested in

Unitary transformation of general nonoverlapping-image multimode interference couplers with any input and output ports

Ze-Zheng Li(李泽正), Wei-Hua Han(韩伟华), Zhi-Yong Li(李智勇)
Chin. Phys. B . 2020, 29(1): 014206 . **doi:** 10.1088/1674-1056/ab5783

Acquisition performance analysis for intersatellite optical communications with vibration influence

Jing Ma(马晶), Gaoyuan Lu(陆高原), Siyuan Yu(于思源), Liying Tan(谭立英), Yulong Fu(付玉龙), Fajun Li(黎发军)
Chin. Phys. B . 2020, 29(1): 014205 . **doi:** 10.1088/1674-1056/ab577e

Compact and high-efficient wavelength demultiplexing coupler based on high-index dielectric nanoantennas

Jingfeng Tan(谭敬丰), Hua Pang(庞画), Fengkai Meng(孟凤凯), Jin Jiang(蒋进)
Chin. Phys. B . 2018, 27(9): 094217 . **doi:** 10.1088/1674-1056/27/9/094217

Crosstalk analysis of silicon-on-insulator nanowire-arrayed waveguide grating

Kai-Li Li(李凯丽), Jun-Ming An(安俊明), Jia-Shun Zhang(张家顺), Yue Wang(王玥), Liang-Liang Wang(王亮亮), Jian-Guang Li(李建光), Yuan-Da Wu(吴远大), Xiao-Jie Yin(尹小杰), Xiong-Wei Hu(胡雄伟)
Chin. Phys. B . 2016, 25(12): 124209 . **doi:** 10.1088/1674-1056/25/12/124209

Turbulence mitigation scheme based on multiple-user detection in an orbital-angular-momentum multiplexed system

Li Zou(邹丽), Le Wang(王乐), Sheng-Mei Zhao(赵生妹), Han-Wu Chen(陈汉武)
Chin. Phys. B . 2016, 25(11): 114215 . **doi:** 10.1088/1674-1056/25/11/114215

High common mode rejection ratio InP 90° optical hybrid in ultra-broadband at 60 nm with deep-rigded waveguide based on ×4 MMI coupler*

Zi-Qing Lu(陆子晴)[1,2], Qin Han(韩勤)[1,2,3,†], Han Ye(叶焓)[1,2], Shuai Wang(王帅)[1,2], Feng Xiao(肖峰)[1,2], and Fan Xiao(肖帆)[1,2]

[1] *State Key Laboratory on Integrated Optoelectronics, Institute of Semiconductors, Chinese Academy of Sciences, Beijing* 100083, *China*
[2] *Center of Materials Science and Optoelectronics Engineering, University of Chinese Academy of Sciences, Beijing* 100049, *China*
[3] *School of Electronic, Electrical and Communication Engineering, University of Chinese Academy of Sciences, Beijing* 100049, *China*

(Received 17 December 2019; revised manuscript received 26 December 2019; accepted manuscript online 1 March 2020)

An InP optical 90° hybrid based on a ×4 MMI coupler with a deep ridged waveguide is designed and fabricated. The working principle of the 90° hybrid is systematically introduced. Three-dimensional beam ropagation method (3D BPM) is used to optimize the structure parameters of the 90° hybrid. The designed compact structure is demonatrated to have a low excess loss less than −0.15 dB, a high common mode rejection ratio better than 40 dB, and a low relative phase deviation less than ±2.5°. The designed hybrid is manufactured on a sandwitched structure deposited on an InP substrate. The measured results show that the common mode rejection ratios are larger than 20 dB in a range from 1520 nm to 1580 nm. The phase deviations are less than ±5° in a range from 1545 nm to 1560 nm and less than ±7° across the C band. The designed 90° optical hybrid is suitable well for realizing miniaturization, high-properties, and high bandwidth of coherent receiver.

Keywords: 90° hybrid, ×4 MMI coupler, deep ridge, high common mode rejection ratio

PACS: 42.79.Sz, 42.25.Hz, 42.79.Gn, 42.82.Fv **DOI:** 10.1088/1674-1056/ab7b52

1. Introduction

During the past few years, real-time coherent optical transmission systems have attracted wide attention due to the potential advantages in large capacity and long-haul transmission. Owing to the quadrature phase shift keying (QPSK) modulation technique, the real-time coherent optical transmission systems greatly reduce the transmission loss per bit, thereby improving the data transmission efficiency.[1–10] Besides, the coherent transmission system offers the more choices of the data transmission rates which are selected by software.[11–14] Therefore, the real-time coherent optical communication technology has been universally recognized as a preferable choice to improve the transmission speed up to 400 Gb/s and more in the industry. The real-time coherent optical transmission system consists of a QPSK transmitter combined with coherent detection and real-time electronic processing circuit. As a key component of the coherent detection, the performance of the 90° optical hybrid is critically important.[15–25] With two pairs of balanced photodetectors (PDs),[26–31] which are based on photoelectricity transformation mechanism, the phase information of the signal light can be demodulated.

This work provides support for a C band real-time coherent optical transmission system in our future work. The InP is considered as a promising platform for photonic integrated circuits (PIC) as PICs can be fabricated in state-of-the-art foundries. The InP based 4 × 4 MMI 90° optical hybrid can offer more smaller footprints in packaging and eliminate complicated alignments in assembly process. Thus, an InP 90° hybrid based on a 4 × 4 MMI coupler was chosen in our previous work.

In this paper, an InP optical 90° hybrid based on a 4 × 4 MMI coupler is designed, fabricated, and analyzed. The self-imaging principle of the 90° hybrid is introduced in Section 2. Three-dimensional beam propagation method (3D BPM) is used to simulate and optimize the field distribution in the hybrid in Section 3. The simulation results show a low excess loss (< 0.2 dB), a high common mode rejection ratio (CMRR) (> 40 dB) and a low relative phase deviation (< 2.5°) across the full C-band. The fabrication details are described in Section 4 with measurement results and analysed in Sections 5 and 6. The measurement results show that a high CMRR of the fabricated 90° hybrid is better than 25 dB in a range from 1520 nm to 1580 nm and low relative phase deviations are less than 5° in a range from 1545 nm to 1560 nm and less than 7° across the C-band, which is suitable for coherent receiver by monolithic integrating balanced detectors. The inaccuracy of the MMI coupler width is analyzed for device performance degradation. Introducing a gradual change in the width of the

*Project supported by the National Key Research and Development Program of China (Grant No. 2016YFB0402404), the Beijing Natural Science Foundation, China (Grant No. 4194093), and the National Natural Science Foundation of China (Grant Nos. 61635010, 61674136, and 61435002).

†Corresponding author. E-mail: hanqin@semi.ac.cn

© 2020 Chinese Physical Society and IOP Publishing Ltd

MMI couplers into the lithography process could be helpful in solving this problem. Finally, some conclusions are drawn from the present syudy in Section 7.

2. Device concept

2.1. Self-imaging principle

Based on the self-imaging principle,[32–34] in the MMI region, the propagation constant β_m for mode m can be obtained by solving the waveguide dispersion equation and expressed as follows:

$$\beta_m \approx k_0 n_{\rm f} - \frac{(m+1)^2 \pi^2}{2k_0 n_{\rm f} W_{\rm em}^2}, \tag{1}$$

where k_0 is the wave vector in vacuum, with $k_0 = 2\pi/\lambda_0$, $n_{\rm f}$ is the effective refractive index of the ridge waveguide, and $W_{\rm em}$ is the effective width for mode m by taking into account the lateral extension depth of each mode field. This expression can be further simplified by replacing the effective width $W_{\rm em}$ by MMI coupler width W, which is resonable for ridge waveguides with high lateral index contrast. Thus, ignoring the Goos–Hähnchen effect,[35] the beat length which is defined as the propagation length difference between the two lowest-order mode can be expressed as

$$L_\pi = \frac{\pi}{\beta_0 - \beta_1} \cong \frac{4 n_{\rm f} W^2}{3\lambda}, \tag{2}$$

where β_0 and β_1 are the propagation constant of the fundamental mode and the first order mode, λ is the operating wavelength of the input light which is set to be around 1550 nm. For a 4×4 MMI coupler, the first 4-fold image appears at the MMI region length of

$$L = 3L_\pi/4. \tag{3}$$

Therefore, if the effective refractive index and the operating wavelength are known, then the MMI region length is a nonlinear function of width. The image points are more sensitive to the width of the MMI coupler.

2.2. 90° hybrid based on a 4×4 MMI coupler

The structure of the key component 4×4 MMI coupler is shown in Fig. 1, which contains four input ports 1/3 in region I, a multimode waveguide in region II, and four output channels 1/2/3/4 in region III. Taper waveguides are adopted to convert spot size.

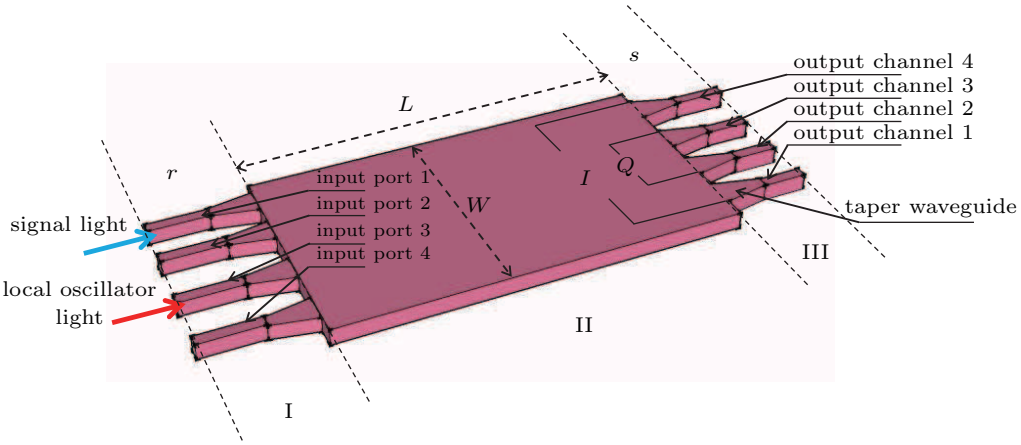


Fig. 1. Structure of 90° hybrid based on 4×4 MMI coupler.

Assuming that the 90° hybrid is ideal, there are no defects nor impurity scattering inside the waveguide. The 90° hybrid works in the transverse electric (TE) mode. When the signal and local oscillation light are inputted simultaneously, the output power at channel 1/2/3/4 can be expressed as

$$I = I_1 + I_2 + 2\sqrt{I_1 I_2}\cos(\Delta\psi + \Delta\phi_s). \tag{4}$$

Here, I_1 and I_2 are the intensity of the signal light and the local oscillation light, respectively; $\Delta\psi$ is the relative phase difference between the signal light and local oscillation light at input port; $\Delta\phi_s$ is the relative phase difference at the output channel s, which is the phase shift between signal light and local oscillation light during propagation in the MMI region, with $\Delta\phi_s = \Delta\phi_{r_s s} - \Delta\phi_{r_{\rm LO} s}$, $\Delta\phi_{r_s s}$ being the phase difference of the signal light between the input port r_s and output channel s, and $\Delta\phi_{r_{\rm LO} s}$ being the phase difference of the local oscillation light between the input port $r_{\rm LO}$ and output channels s, r, and s being the location of the input port channel and output channel, respectively. When the length of the MMI coupler satisfies the condition that the 4-fold image appears, the relative phases between the input port channel and output channel are summarized in Table 1.

For the 90° hybrid application, the input ports of the two input light signals are not arbitrary. The input ports of the signal light and local oscillation light should make the phase diversity $\Delta\phi_s$ of the four output channels are perpendicular to each other on the constellation diagram. The constellation diagram is shown in Fig. 2, in which the signal light and local

oscillation light are launched into input ports 1 and 3. Therefore the locations of the two input ports, which satisfy the requirement for 90° hybrid, can be calculated from Table 1. The input ports 1 and 2 or 1 and 3 or 2 and 4 or 3 and 4 satisfy this condition. Considering the mode crosstalk between the input waveguides, using input ports 1 and 3 or 2 and 4 can effectively avoid the effect of this crosstalk.

Table 1. Theoretical relative phase between input port channel and output channel in 4×4 MMI coupler.

S	1	2	3	4
ϕ_{1s}	π	$3\pi/4$	$-\pi/4$	π
ϕ_{2s}	$3\pi/4$	π	π	$-\pi/4$
ϕ_{3s}	$-\pi/4$	π	π	$3\pi/4$
ϕ_{4s}	π	$-\pi/4$	$3\pi/4$	π

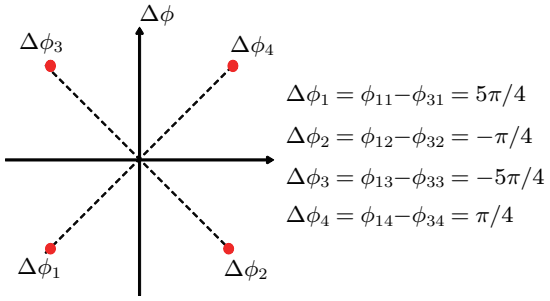


Fig. 2. Constellation diagram of phase difference at four output channels 1/2/3/4, showing that signal light and local oscillation light are launched into ports 1 and 3.

In this work, we choose input ports 1 and 3 as the input ports of the 90° hybrid. If the relative phase difference $\Delta\psi$ between the input ports 1 and 3 are $3\pi/4$, $\pi/4$, $-\pi/4$, and $-3\pi/4$, the cosine term in Eq. (4) can be expressed as

$$\begin{bmatrix} \cos\left(\Delta\phi_1+\frac{3\pi}{4}\right) & \cos\left(\Delta\phi_1+\frac{\pi}{4}\right) & \cos\left(\Delta\phi_1-\frac{\pi}{4}\right) & \cos\left(\Delta\phi_1-\frac{3\pi}{4}\right) \\ \cos\left(\Delta\phi_2+\frac{3\pi}{4}\right) & \cos\left(\Delta\phi_2+\frac{\pi}{4}\right) & \cos\left(\Delta\phi_2-\frac{\pi}{4}\right) & \cos\left(\Delta\phi_2-\frac{3\pi}{4}\right) \\ \cos\left(\Delta\phi_3+\frac{3\pi}{4}\right) & \cos\left(\Delta\phi_3+\frac{\pi}{4}\right) & \cos\left(\Delta\phi_3-\frac{\pi}{4}\right) & \cos\left(\Delta\phi_3-\frac{3\pi}{4}\right) \\ \cos\left(\Delta\phi_4+\frac{3\pi}{4}\right) & \cos\left(\Delta\phi_4+\frac{\pi}{4}\right) & \cos\left(\Delta\phi_4-\frac{\pi}{4}\right) & \cos\left(\Delta\phi_4-\frac{3\pi}{4}\right) \end{bmatrix} = \begin{bmatrix} 1 & 0 & -1 & 0 \\ 0 & 1 & 0 & -1 \\ 0 & -1 & 0 & 1 \\ -1 & 0 & 1 & 0 \end{bmatrix}. \tag{5}$$

In Eq. (5), each column of the matrix corresponds to the power enhancement factors for the four output channels in order. The phase information carried in the signal light can be demodulated from the output power. The output channels 1 and 4 receive the in-phase information of the QPSK signal, which is called in-phase channel (I-channel). The output channels 2 and 3 receive the quadrature information of the QPSK signal, which is called quadrature channel (Q-channel). By further integrating two pairs of balanced photodetectors at the output ports 1, 4 and 2, 3, the photo-generated currents are detected and the corresponding phase information could be demodulated.

3. Device design

In this work, a 90° hybrid based on 4×4 MMI coupler is designed for TE mode at C band (1530 nm–1565 nm). The mode field distribution is simulated by the BPM module of commerical soft called Rsoft. A deep ridge waveguide is adopted and the MMI region length was optimized.

3.1. Deep-ridge waveguides

In this research, a deep ridge waveguide with InP–InGaAsP–InP structure is designed as shown in Fig. 3(a). The cap layer is InP ($n = 3.17$) with a thickness of 1.5 μm, and the core layer is InGaAsP ($n = 3.25$) with a thickness of 0.5 μm.

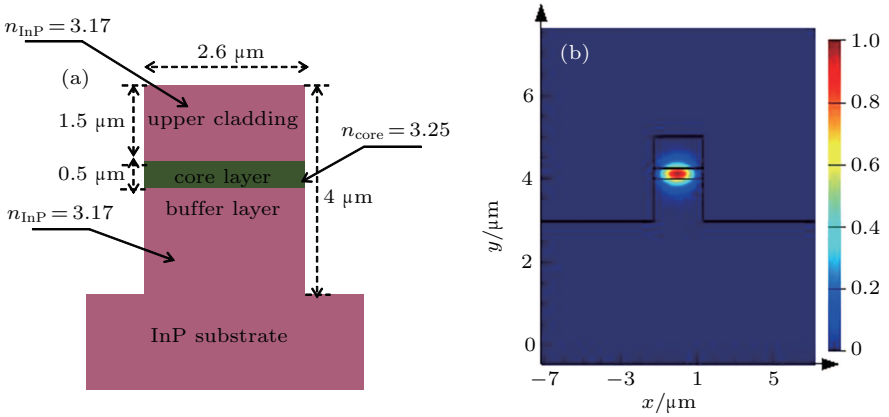


Fig. 3. (a) Cross section and (b) TE mode field distribution of deep ridge InP–InGaAsP–InP access waveguide.

As shown in Fig. 4, only the modes with mode refractive index greater than cladding refractive index can propagate stably in the waveguide, and only single mode appears on the condition that the waveguide width is less than 3.7 μm. The two refractive index curves of TE_0 and TM_0 intersect at 2.6 μm, and the polarization insensitivity can be achieved for the single mode waveguide in this width. Thus, the width of the single mode waveguide is set to be 2.6 μm. The mode refractive index of the access waveguide (TE mode), $n_f = 3.18$, is calculated by the commercial software Lumerical-MODE solution based on finite difference eigenmode (FDE) solver. The TE mode filed distribution is shown in Fig. 3(b).

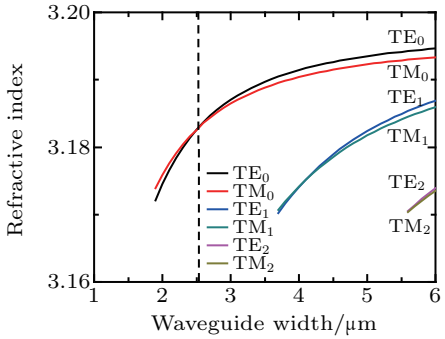


Fig. 4. Mode refractive indices *versus* deep ridge waveguide width at 1550 nm.

3.2. 4×4 MMI coupler

Based on the designed deep ridge waveguide structure, the parameters of the MMI structure were designed. Equation (3) is used to roughly estimate the length of the MMI coupler. Considering the miniaturization and performance, the width of the MMI is set to be 20 μm. The length is 840 μm approximately for the TE mode. The optimal length should be given by simulation.

When the light is inputted from input port 1 or 3, the hybrid uniformly separates the light into four beams acting as a 6-dB power splitter, as shown in Figs. 5(a) and 5(b). If signal light and local oscillation light are inputted simultaneously, the light will interfere with each other at the multimode waveguide, and the output power for each of the four output channels will oscillate with the phase difference between the two input light beams. The simulation results are shown in Fig. 5(c). The output power distribution changes with the relative phase difference as equation (5) predicts. Figure 6 shows the influences on the output power of the length and width of the MMI region. Balance of the output power among four output channels is an important reference which is a standard for evaluating the 90° hybrid performance. According to Fig. 6, the optimal length and width of MMI coupler, which can be obtained from the balance parameter, are 842 μm and 20 μm, respectively. Comparing Fig. 6(a) with Fig. 6(b), the 4×4 MMI coupler is more sensitive to the width as indicated by Eqs. (2) and (3). When the length is larger than 835 μm and less than 845 μm, the power of the four output channels are still well-balanced, which is critical to the hybrid performance. However, when the width is less than 19.9 μm and greater than 20.1 μm, the power values of the four output channels become imbalanced quickly.

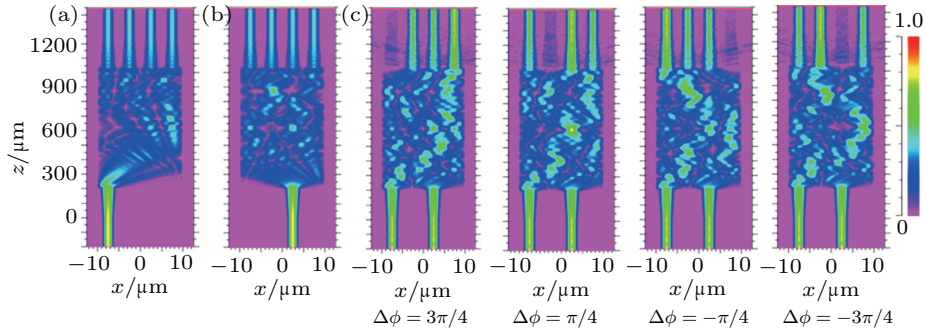


Fig. 5. Field distribution of 90° hybrid for single input at (a) port 1 and (b) port 3, and (c) for two input ports with different phase differences.

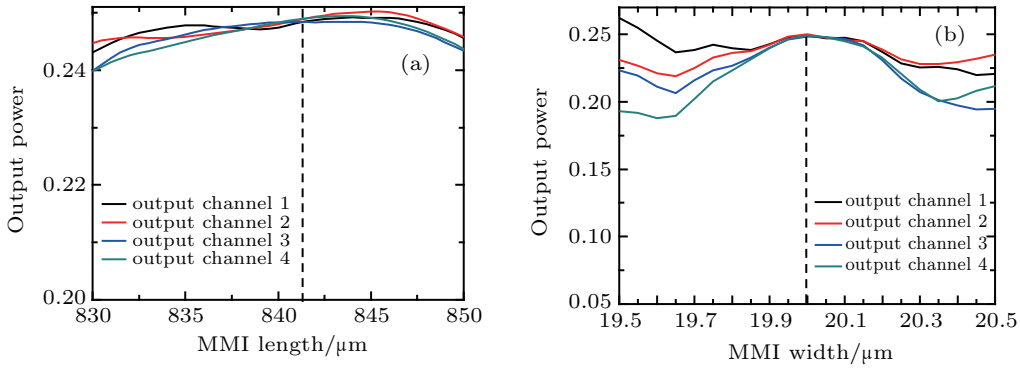


Fig. 6. Simulated output power of hybrid on different (a) lengths and (b) widths of MMI.

The imbalance is an important characteristic for MMI coupler. The common-mode rejection ratio (short as CMRR) represents the output power balance of the I/Q channel which can be expressed as $-20\log(|p_1-p_4|/|p_1+p_4|)/-20\log(|p_2-p_3|/|p_2+p_3|)$, where p_1, p_2, p_3, and p_4 are the powers of the output channels 1, 2, 3, and 4 respectively. The optical internetworking forum (OIF) standard of the coherent communication demands that the CMRR of the I/Q channel be 20 dB better than the C band. In Fig. 7, the simulated CMRRs of I/Q channels are better than 40 dB across the C band, when either port 1 or port 3 is treated as the input channel.

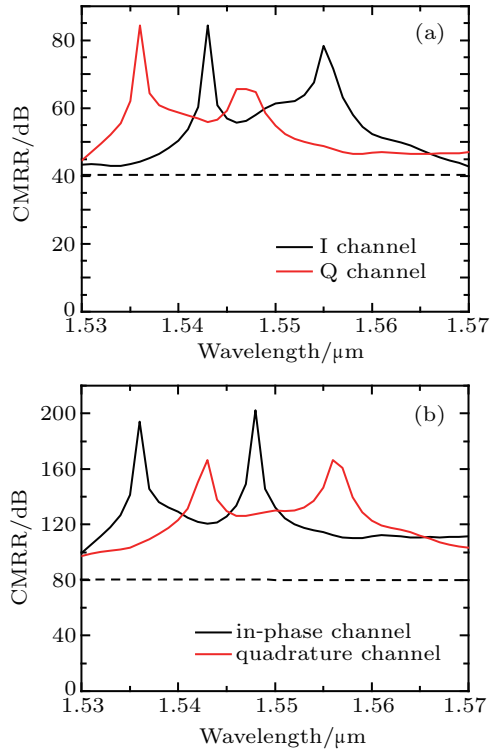


Fig. 7. Simulated CMRR of hybrid launched by (a) input port 1 and (b) input port 3.

The excess loss is calculated for each output channel across the C band. As shown in Fig. 8, the loss of designed 90° hybrid is less than 0.3 dB from 1530 nm to 1570 nm only caused by modes conversion.

To ensure that the hybrid can effectively operate across the full C band, the quadrature phase relationship of output channels needs investigating precisely. For an ideal 90° hybrid, when the signal light and local oscillation light are incident into the access waveguide simultaneously, the theoretical relative phase offsets of channel 1 to 2, 3, and 4, namely $\Delta\varphi_{\mathrm{ch2-ch1}}$, $\Delta\varphi_{\mathrm{ch3-ch1}}$, and $\Delta\varphi_{\mathrm{ch4-ch1}}$ are $-\pi/2$, $\pi/2$, and π, respectively. The phase deviation which is defined as the deviation of the measurement values from the ideal relative phase of the four output channels can be calculated from[19]

$$\frac{\mathrm{FSR}_1}{\Delta\lambda_N}=\frac{2\pi}{\Delta\varphi_N+\Delta\phi_{\mathrm{ch}N-\mathrm{ch1}}}, \tag{6}$$

where FSR_1 is the FSR of channel 1 (Ch-1); $\Delta\emptyset_{\mathrm{ch}N-\mathrm{ch1}}$ and $\Delta\lambda_N$ $(N=2,3,4)$ are the theoretical relative phase offsets and wavelength differences between the peaks of channel 2 (Ch-2) to 1, channel 3 (Ch-3) to 1, and channel 4 (Ch-4) to 1 in the range of FSR_1. OIF standard demands that the phase deviation should remain between ±5° over the C band. Figure 9 shows the simulated phase deviation of our designed 90° hybrid. It is less than ±2.5° over the full C band, which verifies that our design can achieve a desired relative phase deviation level.

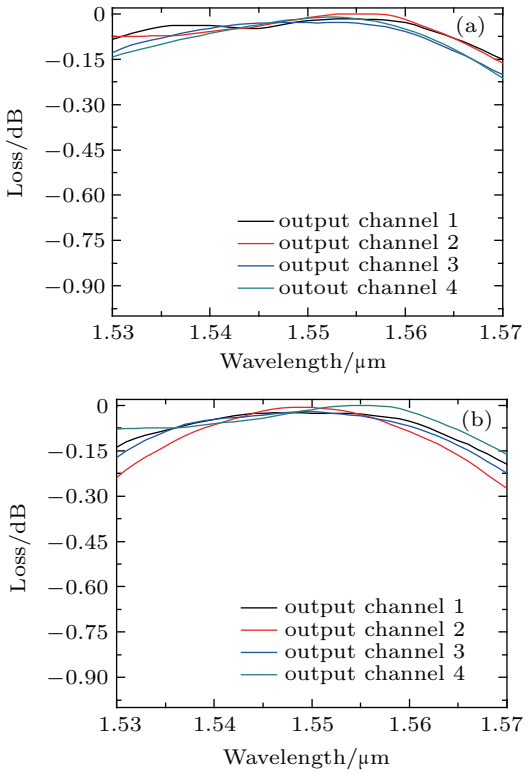


Fig. 8. Simulated excess loss of hybrid launched by (a) input port 1 and (b) input port 3.

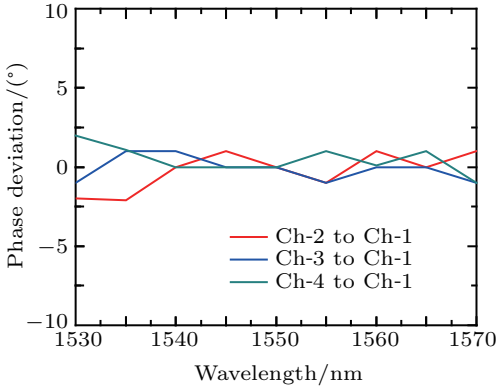


Fig. 9. Simulated phase deviation of designed 90° hybrid.

4. Fabrication

The optimized optical 90° hybrid was fabricated in our processing platform. The waveguide layers are grown on InP substrate by metal–organic chemical vapor deposition (MOCVD). An InP buffer layer was deposited prior to

core layer. The plasma-enhanced chemical vapor deposition (PECVD) was used to deposit a 1-μm-thick silicon dioxide film on the sandwiched structure as a hard mask. Ultra-violet lithography technology was used to define the mask pattern. Then the processes of SiO_2 etching and InP etching were easily performed by the inductively coupled plasma (ICP) etching. Here the InP etching depth was 4 μm. Finally, a SiO_2 layer of 1-μm-thick was deposited on the wafer by PECVD technology in order to protect the device from being influenced externally.

Figure 10 shows the schematic and the scanning electron microscope (SEM) micrograph of the fabricated 90° hybrid. To evaluate the phase relation of the 90° hybrid, a Mach–Zehnder (MZ) delay interferometer was added in the front of the 90° hybrid as shown in Fig. 10(a). The length difference of the delay line is 172 μm, and the free spectral range (FSR), which reflects the oscillation period of the transmission spectrum, is 548 GHz. The radius of the bend waveguide is designed to be 500 μm in order to reduce the waveguide bending loss. Linear taper waveguides from 2.6 μm to 3.7 μm in width were used to connect the access waveguide to the MMI region to improve the coupling efficiency. In order to evaluate the CMRR of this device, several 90° hybrids without MZI were also fabricated on the same wafer.

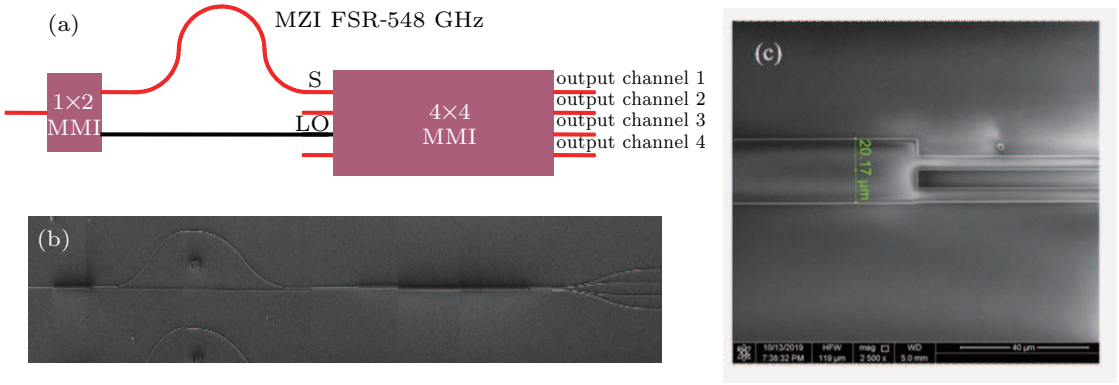


Fig. 10. (a) Schematic diagram and (b), (c) SEM imagings of fabricated 90° hybrid.

5. Measurement and result analysis

The bench setting up for testing the fabricated 90° hybrid is shown in Fig. 11. Polarization-maintaining fibers (PMF) served as optical connecting and chip coupling. The light source wavelength launched from a tunable laser was tuned from 1500 nm to 1600 nm. The polarization of the beam was aligned to TE via a polarization controller (PC). The fused tapering fiber was aligned to the device inputs precisely by means of a six-dimensional coupling system. The coupling efficiency of about 20% was obtained experimentally. The output signal was separated into two beams by using a beam splitter (BS). One beam was incident on the optical power meter to optimize the coupling efficiency and the other one went into the optical spectrometer to measure the spectral response of the fabricated 90° hybrid. In order to avoid being influenced by the external pressure which existed in fiber holder in the polarization state, a splitting prism was used to check the polarization state of the incident light. By rotating the fiber holder, the beam intensity through the prism achieved the highest value, which indicated that the output light from the fiber is TE mode.

The relative phase difference between the signal light and local oscillation light varies with the laser wavelength so that the power of the four output channels varies periodically. One oscillating period corresponds to a 360°-phase shift. According to the offset of the output waveform, the phase deviation of the hybrid can be calculated. The measured transmission spectra of the fabricated 90° hybrid are shown in Fig. 12. Among the four output channels, the orthogonal phase relationship can be clearly observed. The periodic weak oscillations in the measured spectra is probably due to the reflectivity from two ends of the coupling system.

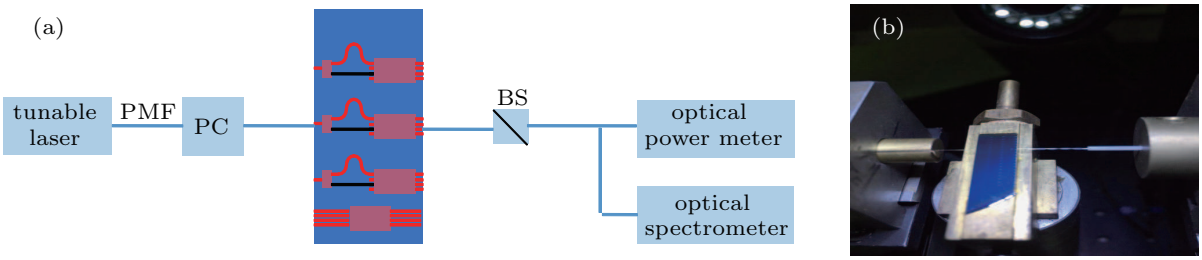


Fig. 11. (a) Measurement instrument and (b) coupling system for testing performance of fabricated 90° hybrid.

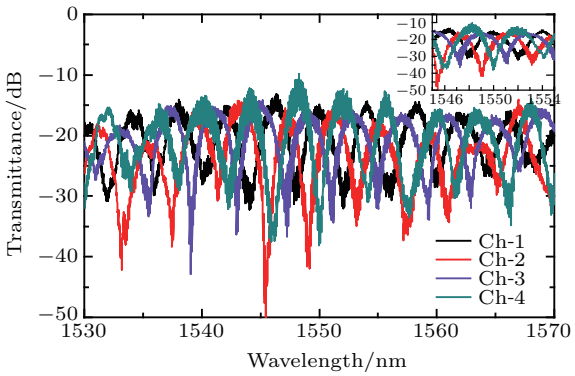


Fig. 12. Measured response spectra of fabricated 90° hybrid.

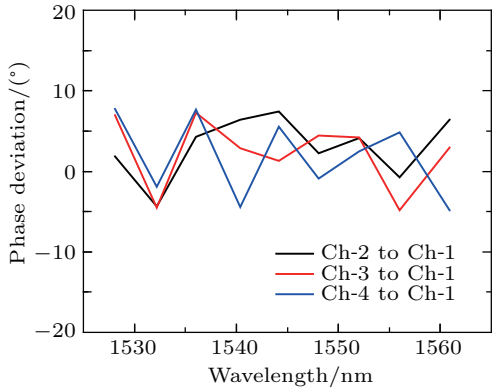


Fig. 13. Calculated relative phase deviation ($\Delta\phi$) of 90° hybrid.

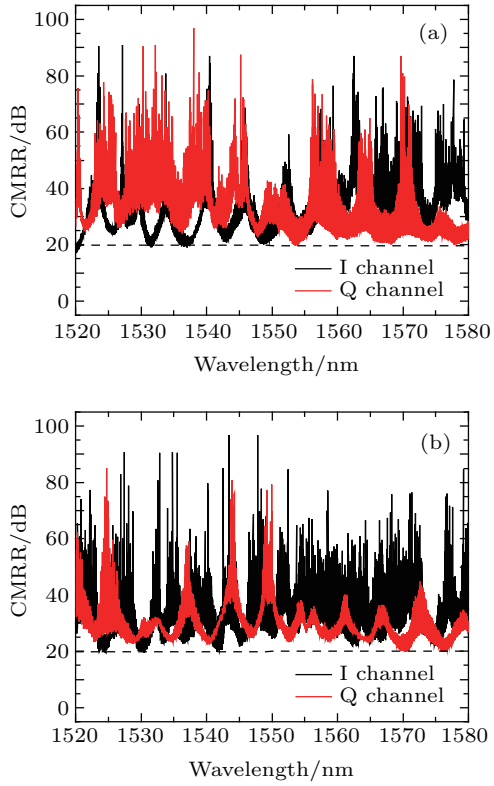


Fig. 14. Measured CMRRs for In-phase channels and quadrature channels of (a) input port 1 and (b) input port 3.

The phase deviation $\Delta\phi$ can be calculated from the wavelength shift of the measured spectral response. Figure 13 shows the calculated relative phase deviation of the fabricated 90° hybrid, which is less than 5° in a range from 1545 nm to 1560 nm and less than 7° over the whole C band. The measured results are slightly worse than the simulated results, probably due to the MMI region width deviation from the design value.

The 90° hybrid without the MZI was measured with the laser beam incident onto input port 1 or 3 of the MMI coupler, and the CMRRs of I/Q channels were calculated and shown in Fig. 14. The CMRRs of the fabricated 90° hybrid are better than 25 dB in a spectral range from 1520 nm to 1580 nm, which exceeds the C band.

6. Error analysis

Refractive index and thickness of material and length and width of MMI coupler are basic parameters of the 90° hybrid. In our laboratory, the refractive index and thickness of core layer can be accurately controlled by MOCVD. For the TE-type hybrid design, the length parameter of the InP MMI coupler was optimized at a width of exactly 20 μm. While the size parameters including width and length are always changed in the lithography and etching process. As analyzed in Section 4, the designed 90° hybrid is highly sensitive to width. Changes in width can yield the deviation of phase information. As can be seen in Fig. 15, the performances of 90° hybrid are highly affected by the width of MMI. When the width change is more than 0.3 μm, the phase deviation rises to more than 10° at 1550 nm. The phase deviation is greater at other wavelengths. From the measured results in Fig. 13, we can see that the performance is deviated from designed value. The fabricated device phase deviation of about 4° can be explained very well from the measured width of 20.18 μm in Fig. 10(c), which corresponds to a phase deviation of about ±4° in Fig. 15. The sensitivity to the processing precision is a common problem of all types of hybrids. In contact exposure, 0.2 μm or more error is always adopted. Considering the limitation of the machining accuracy, a group of hybrids with different widths will be adopted in our future work to approach to the optimal width 20 μm.

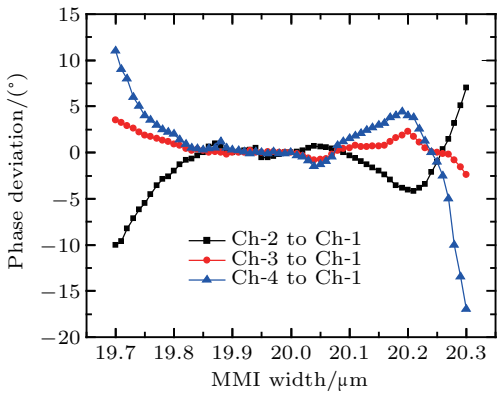


Fig. 15. Simulated phase deviations of InP 90° hybrid varying with MMI width at 1550 nm for Ch-2 to Ch-1, Ch-3 to Ch-1, and Ch-4 to Ch-1, respectively.

7. Conclusions

In this paper, we design, fabricate, and analyze an InP 90° hybrid based on 4×4 MMI coupler with a compact size. An InP/InGaAsP deep ridged waveguide is introduced to reduce the polarization sensitivity and increase the optical confinement factor, and thus improving the device performances. By means of the three-dimensional beam propagation method, the structure parameters of the 90° hybrid is optimized. The simulation results show that the designed 90° hybrid can work very well across the C band. The designed 90° hybrid is fabricated and tested in our laboratory. Experimental results show that the CMRR of the fabricated 90° hybrid is better than 20 dB in a spectrum range from 1520 nm to 1580 nm and the phase deviations are less than $\pm 5°$ in a range from 1545 nm to 1560 nm and less than $\pm 7°$ in the whole C band, which satisfies the requirements for the coherent transmission system. The error analysis can explain the measurement results well. The designed 90° optical hybrid are suitable well for realizing miniaturization, high-properties, and high bandwidth of coherent receiver.

References

[1] Yamamoto Y and Kimura T 1981 *J. Quantum Electron* **17** 919
[2] Kimura T 1987 *J. Lightwave Technol.* **5** 414
[3] Ip E, Lau A P T and Barros D J F 2008 *Opt. Express* **16** 753
[4] Gregory R, Andrew A and Peter J W 2014 *J. Lightwave Technol.* **32** 824
[5] Sun H 2008 *Opt. Express* **16** 873
[6] Pinto A N, Amado S B and Martins C S 2015 *17th International Conference on Transparent Optical Networks (ICTON)*, July 5–9, Budapest, Hungary
[7] Nakazawa M 2010 *Optical and Fiber Communications Reports*, Vol. 6 (Switzerland AG: Springer Nature) pp. 51–80
[8] Yamazaki E, Yamanaka S and Kisaka Y 2011 *Opt. Express* **19** 13179
[9] Deng X, Liu J, Jiao D D, Gao J, Zang Q, Xu G J, Dong R F, Liu T and Zhang S G 2016 *Chin. Phys. Lett.* **33** 114202
[10] Su Y L, Feng H, Hu H, Wang W, Duan T, Wang Y S, Si J H, Xie X P, Yang H N and Huang X N 2019 *Chin. Phys. B* **28** 024216
[11] Shi K, Smyth F and Reid D 2011 *Opt. Commun.* **284** 1616
[12] Yi X, Yu R and Kurumida J 2010 *J. Lightwave Technol.* **28** 587
[13] Meloni G, Paolucci F and Sambo N 2011 *37th European Conference & Exhibition on Optical Communication*, Spetempber 18–22, 2011, Geneva, Switzerland
[14] Chan C K, Jia W and Liu Z 2011 *Asia Communications and Photonics Conference and Exhibition (ACP)*, November 13–16, 2011, Shanghai, China
[15] Patnaik B and Sahu P K 2013 *Int. J. Sig. Imag. Syst. Eng.* **6** 3
[16] Seimetz M and Weinert C M 2006 *J. Lightwave Technol.* **24** 1317
[17] Patrick R, Stefan S and Angela S 2012 *38th European Conference & Exhibition on Optical Communications*, September 16–20, 2012, Amsterdam, Netherlands
[18] Yang W, Yin M, Li Y P, Wang X J and Wang Z Y 2013 *Opt. Express* **21** 28423
[19] Shibata J, Nakao I and Sasai Y 1984 *Appl. Phys. Lett.* **45** 191
[20] Wang Z, Zhai Y, Lu Y, Xu J, Sun X B and Wang J 2018 *Opt. Commun.* **426** 99
[21] Paul M, John M, Graeme B and Nicholas P 2017 *Optical Fiber Communications Coference and Exhibition*, March 19–23, 2017, Los Angeles, CA, USA
[22] Xu L H, Wang Y, Patel D, Morsy-Osman M, Li R, Hui M, Parvizi M, Ben-Hamida N and V plant D 2018 *Optical Fiber Communications Coference and Exposition*, March 11–15, 2018, Sab Duegi, CA, USA
[23] Doerr C R, Gill D M, Gnauck A H, Buhl L L, Winzer P J, Cappuzzo M A, Wong-Foy A, Chen E Y and Gomez L T 2006 *J. Lightwave Technol.* **24** 171
[24] Patrick R, Stefan S, Angela S, Klemens J, Jens S, Dirk T, Patrick D and Mads L N 2012 *Opt. Express* **20** B250
[25] Lars Z, Karsten V, Georg W, Klaus P and Carl M W 2009 *Photon. Technol. Lett.* **21** 143
[26] Deri R J, Pennings E C M, Scherer A, Gozdz A S, Caneau C, Andreadakis N C, Shah V, Curtis L, Hawkins R J, Soole J B D and Song J I 1992 *Photon. Technol. Lett.* **4** 1238
[27] Masaru T, Yoshihiro T and Shoichi O 2013 *39th European Conference and Exhibition on Optical Communication* (ECOC 2013), September 22–26, 2013, London, UK
[28] Islam M S, Murthy S, Itoh T and Wu M C 2001 *IEEE Trans. Microw. Theory Tech.* **49** 1914
[29] Saif Islam M, Thomas J, Itoh T, Wu M C, Nespola A, Sivco D L and Cho A Y 2002 *J. Lightwave Technol.* **20** 285
[30] Lv Q Q, Pan P, Ye H, Yin D D, Wang Y B, Yang X H and Han Q 2016 *Chin. Phys. B* **25** 038505
[31] Zhang Y, Zuo Y H, Guo J C, Ding W C, Cheng B W, Yu J Z and Wang Q M 2009 *Chin. Phys. B* **18** 2223
[32] Soldano L B and Pennings E C M 1995 *J. Lightwave Technol.* **13** 615
[33] Bachmann M, Besse P A and Melchior H 1994 *Appl. Opt.* **33** 3905
[34] Guo F, Lu D, Zhang R K, Wang H T, Wang W and Ji C 2016 *Chin. Phys. Lett.* **33** 024203
[35] Yu T, Li H, Cao Z, Wang Y, Shen Q and He Y 2008 *Opt. Lett.* **33** 1001